Myelodysplastic syndromes disable human CD271^{+}VCAM1^{+}CD146^{+} niches supporting normal hematopoietic stem/progenitor cells

Yuko Kawano[1,5], Hiroki Kawano[1,2], Dalia Ghoneim[3], Thomas J. Fountaine[1,2], Daniel K Byun[1,2], Mark W. LaMere[1,2], Jason H. Mendler[1,2], TzuChieh Ho[1,2], Noah A. Salama[1,5], Jason R. Myers[3], Siba El Hussein[4], Benjamin J. Frisch[4], John M. Ashton[3], Mitra Azadniv[1,2], Jane L. Liesveld[1,2], Youmna Kfoury[5], David T. Scadden[5], Michael W. Becker[1,2], and Laura M. Calvi[1,2,6]

[1]James P. Wilmot Cancer Institute, University of Rochester School of Medicine and Dentistry, Rochester, NY, USA; [2]Division of Hematology/Oncology, Department of Medicine, University of Rochester School of Medicine and Dentistry, Rochester, NY, USA; [3]Department of Genetics, University of Rochester School of Medicine and Dentistry, Rochester, NY, USA;[4]Department of Pathology and Laboratory Medicine, University of Rochester School of Medicine and Dentistry, Rochester, NY, USA; [5]Center for Regenerative Medicine and MGH Cancer Center, Massachusetts General Hospital, Department of Stem Cell and Regenerative Biology and Harvard Stem Cell Institute, Boston, MA, USA; and [6]Division of Endocrinology and Metabolism, Department of Medicine, University of Rochester School of Medicine and Dentistry, Rochester, NY, USA

Y.K and H.K contributed equally to this study.

Key Points

1. Subsets of human bone marrow derived mesenchymal stromal cells provide differential support of hematopoietic stem and progenitor cells.
2. MDS-derived CD271+VCAM-1+CD146+ mesenchymal stromal cells lose their ability to support hematopoietic stem and progenitor cells.

ABSTRACT

Mesenchymal stem/stromal cells (MSCs) within the bone marrow microenvironment (BMME) support normal hematopoietic stem and progenitor cells (HSPCs). However, the heterogeneity of human MSCs has limited the understanding of their contribution to clonal dynamics and evolution to myelodysplastic syndromes (MDS). We combined three MSC cell surface markers, CD271, VCAM-1 (Vascular Cell Adhesion Molecule-1) and CD146, to isolate distinct subsets of human MSCs from bone marrow aspirates of healthy controls (Control BM). Based on transcriptional and functional analysis, $CD271^{+}CD106^{+}CD146^{+}$ (NGFR+/VCAM1+/MCAM+/Lin-; **NVML**) cells display stem cell characteristics, are compatible with murine BM-derived Leptin receptor positive MSCs and provide superior support for normal HSPCs. MSC subsets from 17 patients with MDS demonstrated shared transcriptional changes in spite of mutational heterogeneity in the MDS clones, with loss of preferential support of

normal HSPCs by MDS-derived NVML cells. Our data provide a new approach to dissect microenvironment-dependent mechanisms regulating clonal dynamics and progression of MDS.

Introduction

The BM microenvironment (BMME) serves as the milieu that maintains normal hematopoiesis via cell-cell interactions and secretory factors[1]. Non-hematopoietic stromal cells including mesenchymal stem/stromal cells (MSCs), osteolineage cells (OLC), and BM-derived endothelial and perivascular cells contribute to regulation of hematopoietic stem cell (HSC) function[2-5]. Dysfunction in some of these populations has been reported to participate in the development of hematological malignancies including myelodysplastic syndrome (MDS) and leukemia[6-9]. We have previously shown in a murine model of MDS that targeting the BMME mitigates MDS associated marrow failure and disease progression, decreasing and delaying the risk of transformation to leukemia[10]. MSCs are a key HSC niche cell population in the BMME. MSCs currently are thought to be a heterogeneous population of non-blood forming stem and progenitor cells with potential to differentiate into multiple cell lineages, including osteoblastic, chondrocytic, and adipocytic cells[11]. Although prior studies and consensus statements have reported surface markers for isolating MSCs[12,13 1], recent findings demonstrated significant

diversity in murine BM stroma populations utilizing single cell RNA-seq (scRNA-seq)[2] not accounted for in the study of human BMME populations. While prospective isolation of murine MSC relies on positive expression of CD51 (Integrin αV)[3] and Sca1 (stem cell antigen-1)[4], cell surface markers available for human MSC that individually enrich for stemness and for HSPC support include CD271/NGFR (Nerve Growth Factor Receptor)[5], CD146 (Melanoma Cell Adhesion Molecule)[19,20], and CD106 (VCAM-1)[6]. Using these markers in combination, we identified two novel subpopulations of MSCs from human BM. Comparison of $CD271^{+}CD106^{+}CD146^{+}$ (NGFR+/VCAM1+/MCAM+/Lin-; **NVML**) cells to $CD271^{+}CD146^{-}$ (NGFR+/Lineage- cells; **NLCs**) demonstrated transcriptional and functional differences. Notably, NVML cells display stem cell characteristics and provide superior support for normal HSPCs. Moreover, NVML cells from a cohort of MDS patients demonstrated conserved loss of HSPC support capacity in spite of clinical and mutational heterogeneity.

Materials and methods

Patients

Seventeen treatment naïve patients with MDS were studied (supplemental Table 1). BM and peripheral blood samples were obtained at presentation to the University of Rochester Medical Center following informed consent under institutional review board-approved protocols. BM aspirates from eight healthy age-matched donors

(Control BM) were obtained after informed consent of an institutional review board-approved protocol as previously described[22].

Mononuclear cell isolation from bone marrow aspirates

As previously described[23], diluted marrow aspirate material was layered with a Ficoll-Paque (GE Healthcare Bio-Sciences AB) gradient and centrifuged. Light density bone marrow (LDBM) cells at the interface were collected, and some were cryopreserved in liquid nitrogen. Control BM for the analysis of CFU-F and *ex vivo* expansion for differentiation capacity and co-culture were freshly processed.

Cell sorting

For transcriptional analysis, cryopreserved LDBM cells were thawed and resuspended in FACS buffer (PBS with 2% FBS) and stained with antibody cocktail (biotin-CD45/CD31/CD235ab) with human IgG-Fc block followed by the incubation with streptavidin-magnetic bead particles (BD Biosciences). Magnetic particles were removed based on the manufacturer's direction. Depleted cells were stained with PerCP-Cy5.5-streptavidin, APC-Cy7-CD34, FITC-CD271, APC-CD106, PE-CD146, and DAPI. Human MSCs were sorted on a FACSAriaⅡ (BD Biosciences) at the University of Rochester Medical Center Flow Core. Sorted cells were submitted to RNA sequencing. For cell culture assays, LDBM cells were stained with APC-Cy7 antibody cocktail (CD45/CD31/CD34) and biotin-CD235ab subsequently stained with APC-Cy7-streptavidin. Cells labeled with APC-Cy7 were

depleted by using anti-APC magnetic beads with auto MACS pro (Miltenyi Biotec). The selected APC-Cy7 negative population was subsequently stained with PE-CD271, PE-Cy7-CD146, and APC-CD106. Antibodies are listed in Supplemental Table1.

Colony forming unit of fibroblast (CFU-F) and cell culture

Sorted MSCs were cultured in αMEM without ascorbic acid (Gibco) supplemented with 10% FBS, 1% P/S on a Collagen-1 coated culture dish in hypoxic conditions (2% O_2). The MSCs were plated at a minimal density of (500 cells/cm^2)[24]. For passaging, cells were washed twice with PBS, detached by incubating each well with TrypLE Express Enzyme (Gibco) at 37ºC for 4-5 minutes. *Ex vivo* expanded MSCs were used at passage 3rd to 6th. CFU-F assays were performed as previously described[7].

Flow cytometry

Analytical flow cytometry were performed on a LSR Fortessa (BD Biosciences) as previously described[10]. Viable cells were isolated based on DAPI. Data analysis was performed using FCS Express version 7 (De Novo Software).

Plate coating with rat Collagen Type I

The tissue culture treated plates were coated with rat tail collagen Type I (Corning) according to the manufacturer's protocol. Briefly, 50 µg/ml of collagen type I

solution was prepared using 0.02 N acetic acid and dispensed in the plates followed by overnight incubation at RT. On the following day, the plates were washed with PBS once and stored at 4ºC.

RNA-seq analysis

Total RNA was extracted from sorted MSCs using the RNeasy Plus Micro Kit (Qiagen) per manufacturer's recommendations. RNA concentration was determined with the NanoDrop 1000 spectrophotometer (NanoDrop) and RNA quality assessed with the Agilent Bioanalyzer 2100 (Agilent). 1ng of total RNA was pre-amplified with the SMARTer Ultra Low Input kit v4 (Clontech) per manufacturer's recommendations. The quantity and quality of the subsequent cDNA was determined using the Qubit Fluorometer (Life Technologies) and the Agilent Bioanalyzer 2100. 150pg of cDNA was used to generate Illumina compatible sequencing libraries with the NexteraXT library preparation kit (Illumina) per manufacturer's protocols. The amplified libraries were hybridized to the Illumina flow cell using the cBot (Illumina) and sequenced with single-end reads of 100 nt on the Illumina HiSeq2500.Raw sequencing files were demultiplexed using bcl2fastq-2.19.0. Quality filtering and adapter removal were performed using FastP-0.20.0. The resulting fastq files were mapped to the hg38 reference genome using STAR aligner version 2.7.0f. Gene-level read quantification was performed with featureCounts on exonic regions based on gencode M31 annotation. Differential expression analysis was performed using

DESeq2-1.22.1 in R version 3.5.1. Differentially expressed genes were selected using a Wald test with adjusted p-value threshold of 0.05. Benjamini-Hochberg multiple test correction was applied to calculate the adjusted p-value. In the differential expression comparison of MDS versus Control BM samples, the NLC and NVML Control samples and the MDS samples were utilized in DESeq2 model building. All regression models were adjusted for sequencing batch. Principal component analysis was performed using the DESeq2 pcaplot function on rLog transformed expression values. Principal component plots were created using pcaExplorer-2.14.2 in R. Heatmaps were generated using pheatmap-1.0.12 on rLog transformed expression values and were scaled by expression value within each row. Gene set enrichment analyses was performed using the enrichR-3.0 R package. We tested for enrichment of both up and down regulated differentially expressed gene sets across terms in the wikiPathways human database version 2019, GO Biological processes version 2018, KEGG pathways human database version 2019, and the ChEA 2016 database. Genelists for Lepr+ MSC associated marker genes were obtained from scRNAseq data as previously published[15].

DNAseq variant analysis

Targeted sequencing analysis of 14 MDS patients BM samples was performed using Illumina TruSight Myeloid Sequencing Panel following the manufacturer's recommendations. Libraries were sequenced on Illumina HiSeq2500 with PER250

to generate mean amplicon coverage depth of 15000X or greater. The threshold for quality control for any mutation identified was minimum of 20X read depth.

Samples were analyzed with the Illumina Basespace TruSeq amplicon workflow-3.0.0 using reference genome hg19. The workflow uses Isas-1.17.9.271+TSAv3, SAMtools-1.2, Isas Smith-Waterman-Gotoh-6.2.1.25 aligner, and Pisces-5.2.1.22 variant caller. Variants were annotated using the Illumina annotation engine-1.5.3.82 with annotation dataset-84.24.36. The readout for identified driver genes for MDS pathology were defined by in-house NGS method of University of Rochester listed in Supplemental Table 4.

MSC differentiation

MSC differentiation assays were performed using standard methodologies previously described[23], and passage 4th to 6th cultured cells were tested. Briefly, for the adipocytic induction, after 90-100% confluence was obtained, fat induction medium containing α-MEM supplemented with 10% FBS and 1% P/S (Gibco), rosiglitazone (10µM; Cayman Chemicals), dexamethasone (1µM; Sigma-Aldrich), isobutyl-1-methylxanthine (IBMX; 25µM; Cayman Chemical) and insulin (0.2unit/ml; Humulin® R; Lilly LLC) were added**.** Induction media were changed after three days and replaced with maintenance media containing insulin (0.2 unit/ml) for 24 hr. This cycle was repeated twice followed by 5 days of maintenance and at day12, cells were fixed and stained with Oil Red O solution (Electron Microscope Sciences).

The percentage of oil Red O-positive cells was manually counted. For the osteogenic induction, after MSC cell confluence reached 70-90% , growth media were replaced with complete mineralizing media (α-MEM with ascorbic acid with 10% FBS , 1% PSG, 10 nM dexamethasone, 100 mM L-ascorbic acid and 10 mM β-glycerophosphate (Sigma-Aldrich). After 14 days of induction, cells were fixed in 10% neutral buffered formalin and stained with Alizarin Red S (Electron Microscope Sciences) Von Kossa solution. Chondrocyte induction was performed with MesenCult^{TM}-ACF media according to the manufacturer's protocol (StemCell Technology). After 21 days of induction, cell pellets were fixed and embedded in Histogel (ThermoFisher Scientific). After embedding in paraffin and sectioning, Alcian-Blue (EMD Millipore) staining for cartilage was performed[25] with nuclear staining of Nuclear Fast Red (R&D).

Light microscopy

Images were taken at RT using CKX41 inverted microscope and DP74 camera with a Cellsens software (all, Olympus).

MSC co-culture to assess colony forming units (CFU-C)

CFU-Cs were assayed as previously described[26]. Cryopreserved LDBM cells from Control BM (1X10^5 cells/well) with MSC monolayers which were 80%-90% confluent. All the cells were collected after trypsinization and then plated to duplicate dishes in MethoCult medium (Stem Cell Technologies, H4534)

supplemented with 3 units/ml of human EPO (Peprotec) and 10 ng/ml of G-CSF (Filgrastim, Millipore Sigma). After the 7-days, Colonies (more than 40 cells per colony) were manually counted.

Statistical analysis

Statistical analyses were performed by using GraphPad Prism software 9 (GraphPad Software). Experiments were repeated at least twice. Data are expressed as mean ± standard error of the mean of the independent biological replicates. Some analyses were made using 2-tailed Student's *t* test, Mann-Whitney nonparametric testing, or 1-way ANOVA with Tukey's multiple-comparisons post-test or corrected method of Benjamini and Yekutieli when appropriate. *P* value less than .05 was considered statistically significant and denoted by asterisks (*$p<0.05$, **$p<0.01$, ***$p<0.001$). RNA sequencing data were adjusted p value(q) less than .05 was considered significant and denoted by asterisks (*$q<0.05$, **$q<0.01$, ***$q<0.001$).

Results

Distinctive transcriptional profiles of novel human bone marrow-derived MSC subsets

After obtaining BM aspirates from eight healthy individual, we developed our sorting platform to prospectively isolate three human BMME stromal cell populations from CD45-/CD34-/CD31-/CD235ab- cells: $CD271^{+}CD146^{-}CD106^{-}$ (NLCs), $CD271^{+}CD146^{+}CD106^{-}$ (NML cells), and $CD271^{+}CD146^{+}CD106^{+}$ (NVML cells) (Figure 1A). Principal component analysis (PCA) of the transcriptomes from each sorted cell population demonstrated that NLCs and NVML cells are clearly distinguishable (Figure 1B), while the transcriptional profile of NML cells overlaps with the two other populations (Supplemental Figure 1A). Similarly, heatmap and hierarchical clustering analyses of differentially expressed genes showed clear separation of the transcriptomes of NLCs and NVML cells (Figure 1C, Supplemental Figure 1B). Together, these data suggest that NVML cells and NLCs represent distinct populations, while NML cells may represent a transitioning population between these two.

To characterize these novel human stromal cell populations, we performed gene ontology analysis, and found that, in NVML cells, pathways associated with stemness and multi-lineage differentiation were up-regulated, while pathways related to DNA/RNA processing were down-regulated (Figure 1D, 1E). Furthermore, expression of *MKI67*, the gene encoding Ki67, a known proliferation marker, was higher with NLCs (Figure 1F). This suggests that NVML cells are more quiescent and multipotent in comparison to NLCs.

Recently the Scadden laboratory employed an unbiased approach to define the cellular taxonomy of murine non-hematopoietic BM niche cells and reported the

transcriptional profile of Leptin receptor (LepR)+ MSCs, an MSC subpopulation critical for HSPC support in mice.[15] Compared to NLCs, NVML cells more closely recapitulated the LepR+ MSC subset identified in Baryawno et al. as shown by expression of key genes including *CXCL12 (SDF-1a)*, KITLG (*Kit ligand*) and *LEPR* (Figure 2A). As expected, the expression of *VCAM1,* the gene that encodes CD106, was increased in NVML cells (Fig. 2A, B). NMVL cells are also likely enriched for human CXCL12 Abundant Reticular (CAR) cells, previously shown to be a critical HSC-supportive population, since NVML have increased expression not only of *CXCL12* but also of the characteristic CAR cell genes *FOXC1* and *EBF3*[27-29](Fig.2A,B). Again suggesting that NML cells represent a transitional stromal cell population, NML cells were distributed randomly amongst other populations in the heatmap (Supplemental Figure 2A). Together, these data suggest that NVML cells are enriched for cells that have the potential to support hematopoietic stem and progenitor cells.

NVML cells are enriched for multipotent stem cells with trilineage differentiation capacity

We next investigated the trilineage differentiation capacity of NVML and NLC populations using *ex vivo* culture. Within the stromal cell pool, NVML cells are relatively rare (Figure 3A), however they have higher CFU-F capacity compared to NLCs (Figure 3B). Transcriptional analysis found that key markers for tri-lineage differentiation potential (osteogenic marker: *SPP1* (Osteopontin), adipogenic

marker: *PPARG*, and chondrogenic marker: *SOX9*) were increased in NVML cells compared to NLCs (Figure 3C). Consistent with this, NVML cells had higher propensity for osteogenic, adipogenic, and chondrogenic differentiation compared to NLCs (Figure 3D-G). These characteristics are compatible with increased multipotentiality and stemness of NVML cells as compared with NLCs.

NVML cells and NLCs differentially support hematopoietic stem and progenitor cells

A key function of MSC niche cells is support of normal adult hematopoiesis. In murine BMME studies, genetic tools and single cell datasets have identified subsets of BM MSCs that support hematopoiesis.[2-5,15,8] Our transcriptional analysis suggest that NVML cells recapitulate the LepR+ MSC subset compared to NLCs[2]. To functionally evaluate the supporting capacity of NVML and NLC populations, we established a growth factor-free co-culture system using each sorted stromal cell subset with normal bone marrow-derived hematopoietic cells (Control BM) (Figure 4A). After 3 days of co-culture, we found that NVML cells provided superior support to Control BM CFU-Cs compared to Control BM cultured alone or with NLCs (Figure 4B). This increased ability of NVML to support HSPCs is consistent with their increased expression of the LepR and of the HSC-supportive ligands *CXCL12 (SDF-1a)*, KITLG (*Kit ligand*) and ANGPT-1 (*Angiopoietin-1*) (Figure 4C). NVMLs also demonstrate increased expression of cytokines that support hematopoietic

progenitors (*CXCL10*, *CCL2*, *CSF1*) (Fig 4C). These data indicate that NVML cells are niche cells for normal HSPCs.

NVML cells are selectively disrupted in the MDS BMME

To characterize the impact of MDS on the NVML and NLC sub-populations of human BM MSCs, we analyzed the transcriptome of NVML cells and NLCs from patients with MDS in comparison with aged-matched Controls. Our MDS patient cohort was clinically and mutationally heterogenous (Supplemental Figure 3, Supplemental Table 2, Supplemental Table 3 and). The transcriptome of NVML cells from MDS patients was more severely disrupted compared to that of NLCs (Figure 5A). Notably, in patients with MDS, the number of differentially expressed genes (DEGs) between NVML cells and NLCs was decreased compared to Control, especially in patients clinically defined as high-risk (MDS-EB) based on the blast percentage in BM or peripheral blood (Figure 5B). These data suggest that, in MDS, these two microenvironmental populations are more similar to each other transcriptionally in spite of being phenotypically distinct. Top up-regulated pathways in MDS-derived NVML cells compared to Controls included DNA/RNA processing and cell cycle (Supplemental Figure 4A, Figure 5C), exemplified by the upregulation of Ki67 expression in NVML cells in MDS compared to Control (Figure 5D). These data suggest that NVML cells from MDS patients lose stemness characteristics. Moreover, MDS-induced changes in the transcriptional profile include evidence of response to increased cellular stress and DNA damage, with

enrichment in cellular senescence and Fanconi anemia pathways in NVML from MDS compared to NVML from Controls (Figure 5C, Supplemental Figure 4C)[31]. Notably, increased senescence has been previously reported in MSCs from MDS patients[6,32,33]. Other significantly upregulated genes in NVML in MDS were related to inflammation and metabolism (Supplemental Figure 4D).

Most of the pathways downregulated in NVML cells from MDS patients were related to cytokine signaling (Supplemental Figure 4B). Importantly, the expression of some of the key HSC-supportive genes such as *CXCL12*, *KITLG* (Kit ligand), *ANGPT-1* (Angiopoietin-1), and others were downregulated in NVML cells from MDS patients (Figure 5E, Supplemental Figure 4E). Collectively, these findings would predict that, in spite of mutational heterogeneity in the MDS cells, NVML cells from MDS patients would have decreased capacity to support normal hematopoietic stem and progenitor cells.

Consistent with the transcriptional analysis, coculture of MDS-derived NVML cells with Control BM demonstrated a 4-fold loss of hematopoietic stem and progenitor support compared to normal NVML (Figure 4B). In fact, NVML from MDS patients did not provide additional HSPC support compared to bone marrow alone, demonstrating MDS-dependent disabling of the HSPC niche. Moreover, compared to NLCs, NVML cells from MDS patients were no longer superior in their support of normal CFU-Cs (Figure 4C). These data suggest that a shared characteristic in the MDS microenvironment, regardless of mutation type, is loss of NVML cell function as supportive niches for normal HSPCs.

Discussion

MSCs are a critical cell component of the BMME and their roles in supporting normal hematopoiesis as well as in myeloid malignancies have been explored mainly using murine models. Recently, human BM- MSCs have emerged as therapeutic tools for a number of diverse applications, including immune remodeling and tissue regeneration, but whether specific MSC-dependent signals contribute to disease progression in myeloid neoplasms remains elusive. An improved understanding of the diversity of BM-MSC subpopulations would significantly aid our ability to define and modulate the role of the BMME in these conditions.

Dissecting the heterogeneity among bone and marrow stromal progenitors has been complicated by the rarity of these populations and limited availability of MSC-specific surface markers. Single cell sequencing analysis provides a promising tool for dissecting this population, but with a rarity of <1%, obtaining enough cells and deep enough reads to distinguish this heterogeneity is near the limit of detection. While this problem remains in murine models, CD271 (NGFR) has more recently been identified in humans as specific to a broad population of bone marrow MSCs. CD271 is a neurotrophic factor receptor known to play a role in neuron development, neuron networking[35] and the repair of skeletal injury[36]. While

expression levels on MSCs vary by report and tissue of origin, CD271 is highly expressed on human MSCs isolated by *ex vivo* culture of plastic-adherent cells and on BM-MSCs[37].

To begin to define the heterogeneity of BM-MSC populations, we combined CD271 with markers previously found to be expressed on human BM-MSCs. CD146 (MCAM) is a receptor for lamininα_4 that is highly expressed in vascular muscle wall cells, endothelial cells and pericytes. $CD271^+CD146^+$ human MSC populations were found to have greater colony forming capacity compared to $CD271^+CD146^-$ populations[24] and to be located in perivascular areas *in vivo*[19]. Since CD106 (VCAM-1) is an adhesion molecule that facilitates interactions with vascular endothelium, we combined these markers with VCAM-1 given the perivascular location of HSC niche cells in murine models, and because previous work showed that enrichment with VCAM-1 within CD271+ BM-MSCs identifies self-renewing cells[21]. Importantly, single cell analysis of CD271+ MSCs has identified similar functional subsets within the MSC population as those we have identified here[38-41]. However, without the ability to identify these subsets immunophenotypically, it is impossible to directly test them functionally *ex vivo*. Here, we demonstrated utilizing three biomarkers including CD271, CD146 and CD106, can provide a novel tool for direct comparative analysis of these populations in human health and disease.

By combining transcriptional profiling with functional assays, we confirmed the heterogeneity of CD271^{+} BM-MSCs and identified CD271^{+}CD146^{+}CD106^{+}, NVML cells, as the subset enriched for stem cell characteristics, as evidenced by a greater colony forming capacity, greater potential for multi-lineage mesenchymal differentiation and increased quiescence.

While there are considerable murine data regarding hematopoietic supportive MSC subsets, human MSC subsets have been difficult to test functionally for hematopoietic support. This is of critical importance, since emerging data strongly suggest that microenvironmental remodeling may contribute to clonal dynamics and evolution to leukemic transformation[42,43]. Our work represents one of the first functional tests on hematopoietic supportive capacity of MSC subset populations.

Our data identify NVML cells as especially supportive of normal HSPCs (Figure 6). Consistent with this, in comparison to NLCs, the transcriptional profiles of NVML cells demonstrate greater overlap with the HSC-supportive murine LepR+ MSCs identified by Baryawno et al. [15], Our analysis confirms that the BM stroma taxonomy identified in this murine study is recapitulated by human MSC subpopulations. The fact that our newly defined human NVML cells are aligned with the well-characterized murine LepR+ MSC population represents a powerful tool to compare the impact of perturbations of the murine BMME to human samples in future prel=clinical studies.

Current strategies assessing functional MSC subsets *ex vivo* rely heavily on proliferative capacity and minor changes in trilineage differentiation capacity[38,44,45]. While these are characteristic functions of MSCs they do not address hematopoietic support. While there is considerable murine data regarding hematopoietic supportive MSC subpopulations[46,47], human subpopulations have been difficult to test functionally. To confirm the identity of human BM-MSCs capable of supporting HSPCs, we established co-culture systems of human NVML and NLC cells in the absence of supplemental cytokines. Notably, our sorting strategy using bone marrow aspirates and *ex vivo* expansion procedures made this functional assay possible. This approach is unique compared to previous studies that rely on obtaining transcriptional information from specific populations of MSCs after *ex vivo* expansion[38,39] and *in vivo* histological evaluation[9] or only utilized *ex vivo* culture using bone fragments rather than BM aspirates[6]. This innovation helps us highlight the supportive role of MSC populations that may at least in part be due to their production of growth factors and cytokines.

Analysis of MSC subsets in a diverse group of MDS patients demonstrates that the transcriptomes of MDS-derived NVML cells share patterns of dysregulated expression despite the mutational heterogeneity of the associated myeloid malignancy. Our transcriptional and functional data demonstrate that MDS-derived NVMLs lose their ability to support normal HSPCs, suggesting that disruption of NVML cells is at least partially responsible for the loss of normal hematopoietic

function common to patients with MDS. We speculate that the loss of supportive niches for normal HSPC combined with the competitive advantage provided by the mutation(s) in the clones would result in acceleration of clonal expansion as a mechanism of evolution from clonal hematopoiesis to MDS and transformation to leukemia. Moreover, since one mechanism of treatment resistance is thought to be the emergence of novel clones, our ability to identify signals in NVML cells that are present in MDS patients with mutational heterogeneity may prove a superior therapeutic strategy that may reverse bone marrow failure while decreasing support of diverse MDS clones. Further studies are needed to define the mechanisms driving NVML dysfunction, however our data suggest that stem cell characteristics of NVML cells are critical for their ability to support HSPCs.

In summary, our study identifies a novel niche cell population in the human bone marrow that preferentially supports normal HSPCs and is disrupted in the setting of MDS (Figure 6), providing a new approach to dissect microenvironment-dependent mechanisms regulating homeostasis of human BMME with implications for clonal dynamics and progression to MDS.

Acknowledgements

The authors would like to thank Lizz LaMere for technical assistance and the University of Rochester Flow Cytometry Core and Genomics Core for their

assistance. Funding for this work was provided by the CTSI Incubator Program, a pilot from the UR Center from Rochester Resource-Based Center for Bone, Muscle and Orthopedic Research (ROCSTARR) to YK (P30AR069655), Overseas Research Fellowship, Japanese Society for the Promotion of Science (JSPS) to YK, R01s AG079556 (to LMC and MWB) and AG076786 (to LMC), the Edward P. Evans Foundation (to LMC), Leukemia & Lymphoma Society (LLS) to MWB and the Wilmot Cancer Institute.

Authorship Contributions

Y. Kawano, H.K., L.M.C., M.W.B., D.G designed the experiments, analyzed the data, interpreted the results and wrote the manuscript. Y. Kawano, H.K., M.A., M.W.L, T.C.H, and D.K.B. performed the experiments. D.T.S. Y.K., T.J.F. J.R.M., J.M.A. and J.L.L. contributed to data interpretation and discussion.

Disclosure of Conflicts of Interest

The authors declare no competing interests.

Correspondence : Laura M. Calvi, M.D, Division of Endocrinology and Metabolism, Department of Medicine, University of Rochester School of Medicine, 601 Elmwood Ave, Box 693, Rochester, NY 14642;

E-mail:laura_calvi@urmc.rochester.edu phone: (585) 275-5011; fax: 585-276-2596

Michael W. Becker, M.D, Division of Hematology/Oncology, Department of Medicine, University of Rochester School of Medicine and Dentistry, Rochester, NY, 14642, E-mail: Michael_Becker@urmc.rochester.edu phone: 585-275-5823 and requests for materials should be addressed to L.M.C. and M.W.B.

Additional information is provided in Supplementary Materials.

Availability of Data and Materials

The datasets used and/or analyzed during the current study are available from the corresponding authors.

References

1. Scadden DT. Nice neighborhood: emerging concepts of the stem cell niche. *Cell*. 2014;157(1):41-50.
2. Calvi LM, Adams GB, Weibrecht KW, et al. Osteoblastic cells regulate the haematopoietic stem cell niche. *Nature*. 2003;425(6960):841-846.
3. Ding L, Saunders TL, Enikolopov G, Morrison SJ. Endothelial and perivascular cells maintain haematopoietic stem cells. *Nature*. 2012;481(7382):457-462.
4. Kunisaki Y, Bruns I, Scheiermann C, et al. Arteriolar niches maintain haematopoietic stem cell quiescence. *Nature*. 2013;502(7473):637-643.
5. Mendez-Ferrer S, Michurina TV, Ferraro F, et al. Mesenchymal and haematopoietic stem cells form a unique bone marrow niche. *Nature*. 2010;466(7308):829-834.
6. Zambetti NA, Ping Z, Chen S, et al. Mesenchymal Inflammation Drives Genotoxic Stress in Hematopoietic Stem Cells and Predicts Disease Evolution in Human Pre-leukemia. *Cell Stem Cell*. 2016;19(5):613-627.
7. Raaijmakers MH, Mukherjee S, Guo S, et al. Bone progenitor dysfunction induces myelodysplasia and secondary leukaemia. *Nature*. 2010;464(7290):852-857.
8. Kode A, Manavalan JS, Mosialou I, et al. Leukaemogenesis induced by an activating beta-catenin mutation in osteoblasts. *Nature*. 2014;506(7487):240-244.
9. Dong L, Yu WM, Zheng H, et al. Leukaemogenic effects of Ptpn11 activating mutations in the stem cell microenvironment. *Nature*. 2016;539(7628):304-308.

10. Balderman SR, Li AJ, Hoffman CM, et al. Targeting of the bone marrow microenvironment improves outcome in a murine model of myelodysplastic syndrome. *Blood*. 2016;127(5):616-625.
11. Kfoury Y, Scadden DT. Mesenchymal cell contributions to the stem cell niche. *Cell Stem Cell*. 2015;16(3):239-253.
12. Kolf CM, Cho E, Tuan RS. Mesenchymal stromal cells. Biology of adult mesenchymal stem cells: regulation of niche, self-renewal and differentiation. *Arthritis Res Ther*. 2007;9(1):204.
13. Lv FJ, Tuan RS, Cheung KM, Leung VY. Concise review: the surface markers and identity of human mesenchymal stem cells. *Stem Cells*. 2014;32(6):1408-1419.
14. Dominici M, Le Blanc K, Mueller I, et al. Minimal criteria for defining multipotent mesenchymal stromal cells. The International Society for Cellular Therapy position statement. *Cytotherapy*. 2006;8(4):315-317.
15. Baryawno N, Przybylski D, Kowalczyk MS, et al. A Cellular Taxonomy of the Bone Marrow Stroma in Homeostasis and Leukemia. *Cell*. 2019;177(7):1915-1932 e1916.
16. Pinho S, Lacombe J, Hanoun M, et al. PDGFRalpha and CD51 mark human Nestin+ sphere-forming mesenchymal stem cells capable of hematopoietic progenitor cell expansion. *J Exp Med*. 2013;210(7):1351-1367.
17. Morikawa S, Mabuchi Y, Kubota Y, et al. Prospective identification, isolation, and systemic transplantation of multipotent mesenchymal stem cells in murine bone marrow. *J Exp Med*. 2009;206(11):2483-2496.
18. Jones EA, English A, Kinsey SE, et al. Optimization of a flow cytometry-based protocol for detection and phenotypic characterization of multipotent mesenchymal stromal cells from human bone marrow. *Cytometry B Clin Cytom*. 2006;70(6):391-399.
19. Tormin A, Li O, Brune JC, et al. CD146 expression on primary nonhematopoietic bone marrow stem cells is correlated with in situ localization. *Blood*. 2011;117(19):5067-5077.
20. Sacchetti B, Funari A, Michienzi S, et al. Self-renewing osteoprogenitors in bone marrow sinusoids can organize a hematopoietic microenvironment. *Cell*. 2007;131(2):324-336.
21. Mabuchi Y, Morikawa S, Harada S, et al. LNGFR(+)THY-1(+)VCAM-1(hi+) cells reveal functionally distinct subpopulations in mesenchymal stem cells. *Stem Cell Reports*;1(2):152-165.
22. Ho TC, LaMere M, Stevens BM, et al. Evolution of acute myelogenous leukemia stem cell properties after treatment and progression. *Blood*. 2016;128(13):1671-1678.
23. Azadniv M, Myers JR, McMurray HR, et al. Bone marrow mesenchymal stromal cells from acute myelogenous leukemia patients demonstrate adipogenic differentiation propensity with implications for leukemia cell support. *Leukemia*. 2020;34(2):391-403.
24. Maijenburg MW, Kleijer M, Vermeul K, et al. The composition of the mesenchymal stromal cell compartment in human bone marrow changes during development and aging. *Haematologica*. 2012;97(2):179-183.
25. Mackay AM, Beck SC, Murphy JM, Barry FP, Chichester CO, Pittenger MF. Chondrogenic differentiation of cultured human mesenchymal stem cells from marrow. *Tissue Eng*. 1998;4(4):415-428.
26. Kawano Y, Fukui C, Shinohara M, et al. G-CSF-induced sympathetic tone provokes fever and primes antimobilizing functions of neutrophils via PGE2. *Blood*. 2017;129(5):587-597.
27. Almubarak A, Lavy R, Srnic N, et al. Loss of Foxc1 and Foxc2 function in chondroprogenitor cells disrupts endochondral ossification. *J Biol Chem*. 2021;297(3):101020.
28. Omatsu Y, Seike M, Sugiyama T, Kume T, Nagasawa T. Foxc1 is a critical regulator of haematopoietic stem/progenitor cell niche formation. *Nature*. 2014;508(7497):536-540.

29. Aoki K, Kurashige M, Ichii M, et al. Identification of CXCL12-abundant reticular cells in human adult bone marrow. *Br J Haematol*. 2021;193(3):659-668.
30. Tikhonova AN, Dolgalev I, Hu H, et al. The bone marrow microenvironment at single-cell resolution. *Nature*. 2019;569(7755):222-228.
31. Rodriguez A, D'Andrea A. Fanconi anemia pathway. *Curr Biol*. 2017;27(18):R986-R988.
32. Chen X, Li N, Weng J, Du X. Senescent Mesenchymal Stem Cells in Myelodysplastic Syndrome: Functional Alterations, Molecular Mechanisms, and Therapeutic Strategies. *Front Cell Dev Biol*. 2020;8:617466.
33. Geyh S, Oz S, Cadeddu RP, et al. Insufficient stromal support in MDS results from molecular and functional deficits of mesenchymal stromal cells. *Leukemia*. 2013;27(9):1841-1851.
34. Tohyama K, Tsutani H, Ueda T, Nakamura T, Yoshida Y. Establishment and characterization of a novel myeloid cell line from the bone marrow of a patient with the myelodysplastic syndrome. *Br J Haematol*. 1994;87(2):235-242.
35. Bibel M, Hoppe E, Barde YA. Biochemical and functional interactions between the neurotrophin receptors trk and p75NTR. *EMBO J*. 1999;18(3):616-622.
36. Deponti D, Buono R, Catanzaro G, et al. The low-affinity receptor for neurotrophins p75NTR plays a key role for satellite cell function in muscle repair acting via RhoA. *Mol Biol Cell*. 2009;20(16):3620-3627.
37. Barilani M, Banfi F, Sironi S, et al. Low-affinity Nerve Growth Factor Receptor (CD271) Heterogeneous Expression in Adult and Fetal Mesenchymal Stromal Cells. *Sci Rep*. 2018;8(1):9321.
38. Oguma Y, Kuroda Y, Wakao S, Kushida Y, Dezawa M. Single-cell RNA sequencing reveals different signatures of mesenchymal stromal cell pluripotent-like and multipotent populations. *iScience*. 2022;25(11):105395.
39. Wang Z, Chai C, Wang R, et al. Single-cell transcriptome atlas of human mesenchymal stem cells exploring cellular heterogeneity. *Clin Transl Med*. 2021;11(12):e650.
40. Wang Z, Li X, Yang J, et al. Single-cell RNA sequencing deconvolutes the in vivo heterogeneity of human bone marrow-derived mesenchymal stem cells. *Int J Biol Sci*. 2021;17(15):4192-4206.
41. Zhang C, Han X, Liu J, et al. Single-cell Transcriptomic Analysis Reveals the Cellular Heterogeneity of Mesenchymal Stem Cells. *Genomics Proteomics Bioinformatics*. 2022;20(1):70-86.
42. Fabre MA, de Almeida JG, Fiorillo E, et al. The longitudinal dynamics and natural history of clonal haematopoiesis. *Nature*. 2022;606(7913):335-342.
43. Mitchell E, Spencer Chapman M, Williams N, et al. Clonal dynamics of haematopoiesis across the human lifespan. *Nature*. 2022;606(7913):343-350.
44. Ghazanfari R, Li H, Zacharaki D, Lim HC, Scheding S. Human Non-Hematopoietic CD271(pos)/CD140a(low/neg) Bone Marrow Stroma Cells Fulfill Stringent Stem Cell Criteria in Serial Transplantations. *Stem Cells Dev*. 2016;25(21):1652-1658.
45. Hou W, Duan L, Huang C, et al. Cross-Tissue Characterization of Heterogeneities of Mesenchymal Stem Cells and Their Differentiation Potentials. *Front Cell Dev Biol*. 2021;9:781021.
46. Lin Q, Wu L, Chatla S, et al. Hematopoietic stem cell regeneration through paracrine regulation of the Wnt5a/Prox1 signaling axis. *J Clin Invest*. 2022;132(12).
47. Szade K, Gulati GS, Chan CKF, et al. Where Hematopoietic Stem Cells Live: The Bone Marrow Niche. *Antioxid Redox Signal*. 2018;29(2):191-204.

FIGURE LEGENDS

Figure 1. NVML cells have distinctive transcriptional profiles compared to NLCs A. Gating strategy for sorting of NLCs and NVML cells population. B. Plot of first (PC1) and second (PC2) principal components from principal component analysis of RNA expression in Control BM samples. Each dot represents an individual patient. NLCs (green) and NVML (blue) samples. C. Hierarchical clustering heat map of differentially expressed genes in NVML cells vs NLCs samples scaled per gene. D. Up-regulated and E. down-regulated gene enrichment results from differentially expressed genes in NVML vs NLC samples. Only the top 30 hits are shown. Circle size represents proportion of differentially expressed genes enriched for that term. F. Enrichment curve of Cell cycle pathway obtained by GSEA analysis in comparison of Control NLC vs NVML transcripts. G. Normalized counts data of *MKI67* (Ki67) of NVML cells and NLCs obtained from RNA seq data analysis. n=8, Min to max, adjusted p(q) is provided. ***: $q<0.001$

Figure. 2 Transcriptional profile of NVML cells is compatible with murine LepR+ MSCs A. Hierarchical clustering heat map of the set of differentially expressed genes from LepR+ MSCs in scRNAseq murine dataset[15] in NVML cells (Blue) vs NLCs (Green) samples scaled per gene. B. Normalized counts data of key transcriptomes represent the characteristics of LepR+ MSC or CAR cells, *VCAM1, FOXC1, EBF3* in comparison of NVML cells and NLCs obtained from RNA seq data analysis. n=8, Min to max, adjusted p(q) was provided. *: q<0.05; **: q<0.01; ***: q<0.001.

Figure. 3 NVML cells show stem cell like characteristics compared to NLCs

A. Sorted cell number per 10 million loading (after negative selection) B. Relative CFU-F number, each dot represents an individual experiment. C. Normalized counts from RNA-seq analyses for tri-lineage differentiation gene markers (osteogenic: osteopontin (*SPP1*), adipogenic: PPAR-γ (*PPARG*), chondrogenic: SOX-9 (*SOX9*) for NVML cells compared to NLCs. D. Representative images of alkaline phosphatase/Von Kossa double staining after osteogenic differentiation of NLCs and NVML cells. Red arrows are pointing mineralizing deposits (black dots) and blue arrow is pointing to alkaline phosphatase positive area (pink region). Mock: normal media not including differentiation factors. Induction: media with differentiation factors (see methods). E. Alcian blue staining of chondrogenic differentiation test. F. Representative images of Oil-Red-O staining (red) of adipogenic differentiation test. G. Quantification of adipogenic induction rate (% of

Oil-Red-O positive cells). n=3-5, Student t-test, mean and SEM or Min to max are provided in A, B and G.*: p<0.05; **: p<0.01; ***: p<0.001. Min to max, adjusted p(q) was provided in C: ns: not significant; *: q<0.05; **:q<0.01.

Figure. 4 NVML cells preferentially support normal hematopoietic stem and progenitor cells A. Schematic representation of experimental procedure of *ex vivo* co-culture of MSCs and hematopoietic cells to evaluate CFU-Cs. B. Normalized count of CFU-Cs normal NLC and NVML alone, Control BM alone (n=11), compared with Control BM supported by NVML cells or NLCs derived from Control BM (control NLC/control NVML) or MDS (MDS NLC/MDS NVML). n=3-4 separate BM-derived MSCs from Control BM or MDS patients. One-way ANOVA with corrected method of Benjamini and Yekutieli, mean and SEM.*: p<0.05; **: p<0.01; ***: p<0.001 C. Normalized counts of key transcriptional markers for hematopoietic support. Min to max, adjusted p(q) are provided. *: q<0.05; **: q<0.01; ***: q<0.001.

Figure. 5 NVML cells from MDS patients are uniquely disrupted transcriptionally and functionally A. Volcano plots based on RNAseq expression of NLCs and NVML cells from MDS compared to Control bone marrow samples. The dashed line marks p-value threshold of 0.05. Significantly up and down-regulated genes with adjusted p-value <= 0.05 are highlighted in red and green respectively. Adjusted p-value was calculated using benjamini-Hochburg correction method. B. Bar plot of number of differentially expressed genes (DEGs) between

NLCs and NVML cells. Red and blue bars indicate the total number of up and down regulated genes, respectively. The striped bars in the MDS low-risk NLC vs NVML and MDS high-risk NLC vs NVML indicated the number of DEGs that overlap with Control NLC vs NVML DEGs. C. Enrichment curve of Cell cycle, Cellular senescence and Fanconi anemia pathways obtained by GSEA analysis in comparison of NVML Control vs MDS. D,E. Normalized counts for transcriptional expression of *MKI67 CXCL12*, *KITLG*, *ANGPT1*, *M-CSF* in Control (Cont) NVML cells vs MDS NVML cells. n=8-10 Min to max, adjusted p(q) or p value from Wald test (p) were provided. *: $q<0.05$; ***: $q<0.001$.

Figure 6 CD271, VCAM-1 and CD146 support normal hematopoietic stem and progenitor cells but are disrupted in myelodysplastic syndromes. Schematic summary of NVML niche cells in normal and MDS bone marrow.

Figure.1

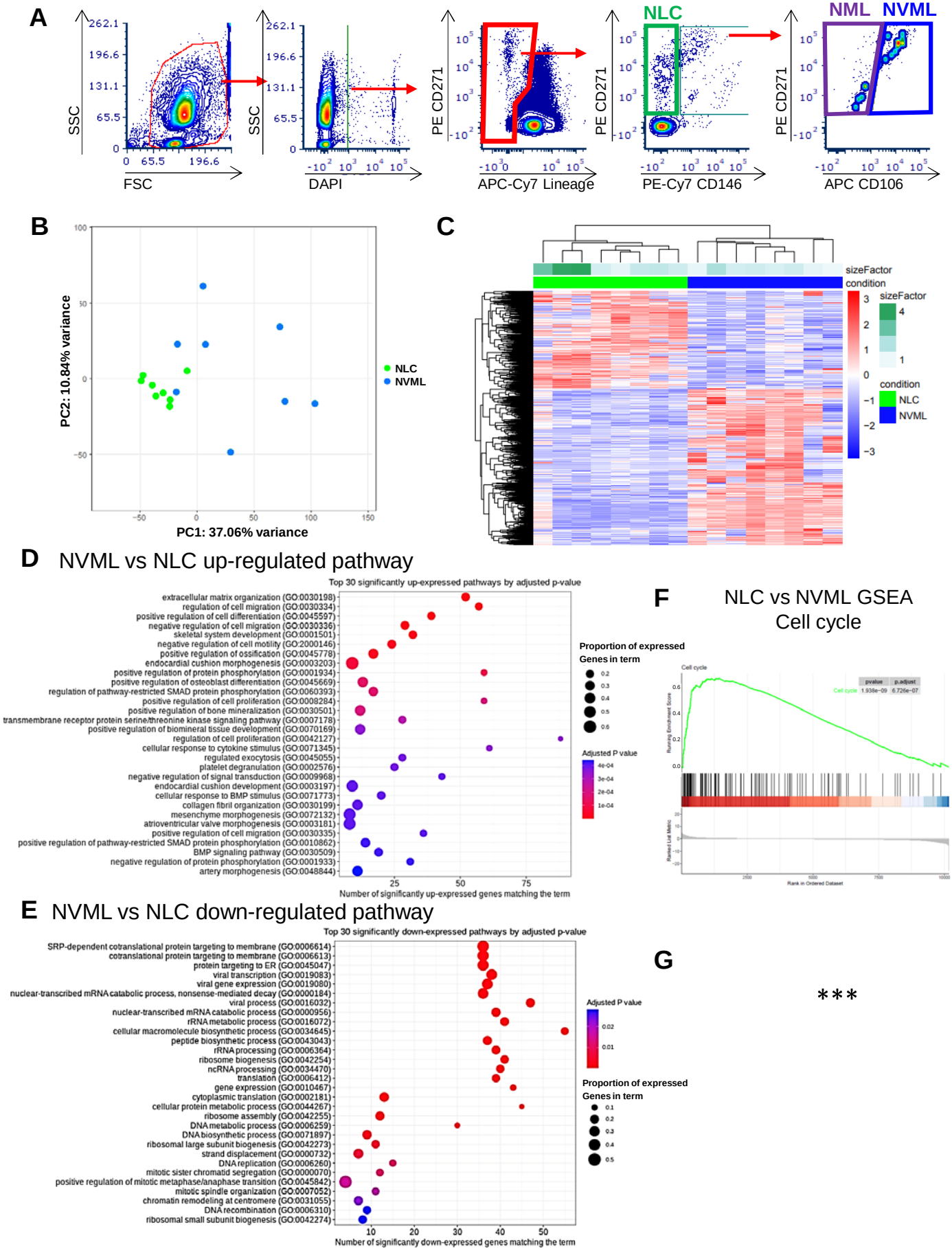
A
SSC
FSC
DAPI
PE CD271
APC-Cy7 Lineage
NLC
PE-Cy7 CD146
NML
NVML
APC CD106
B
PC2: 10.84% variance
PC1: 37.06% variance
NLC
NVML
C
sizeFactor
condition
D NVML vs NLC up-regulated pathway
Top 30 significantly up-expressed pathways by adjusted p-value
Proportion of expressed Genes in term
Adjusted P value
Number of significantly up-expressed genes matching the term
F NLC vs NVML GSEA Cell cycle
Cell cycle
E NVML vs NLC down-regulated pathway
Top 30 significantly down-expressed pathways by adjusted p-value
Adjusted P value
Proportion of expressed Genes in term
Number of significantly down-expressed genes matching the term
G
***

Figure.2

A

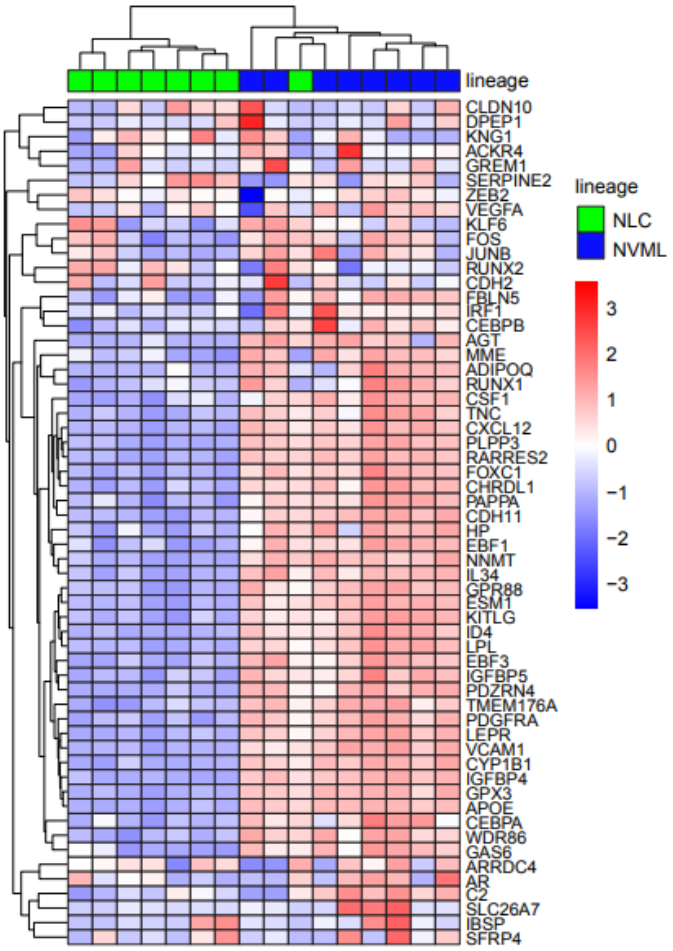
lineage
CLDN10
DPEP1
KNG1
ACKR4
GREM1
SERPINE2
ZEB2
VEGFA
KLF6
FOS
JUNB
RUNX2
CDH2
FBLN5
IRF1
CEBPB
AGT
MME
ADIPOQ
RUNX1
CSF1
TNC
CXCL12
PLPP3
RARRES2
FOXC1
CHRDL1
PAPPA
CDH11
HP
EBF1
NNMT
IL34
GPR88
ESM1
KITLG
ID4
LPL
EBF3
IGFBP5
PDZRN4
TMEM176A
PDGFRA
LEPR
VCAM1
CYP1B1
IGFBP4
GPX3
APOE
CEBPA
WDR86
GAS6
ARRDC4
AR
C2
SLC26A7
IBSP
SFRP4
lineage
NLC
NVML
3
2
1
0
−1
−2
−3

B

*** ** *

Figure.3

A

B

C

ns

**

*

D

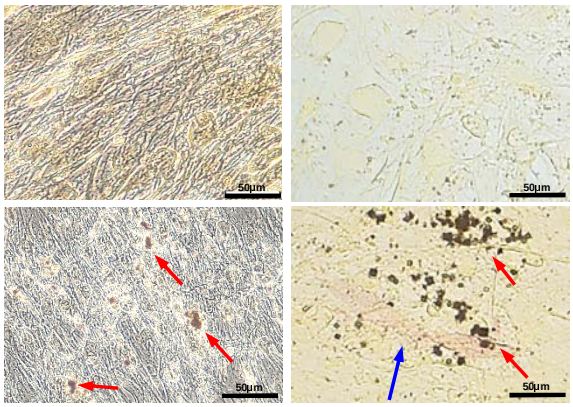

E

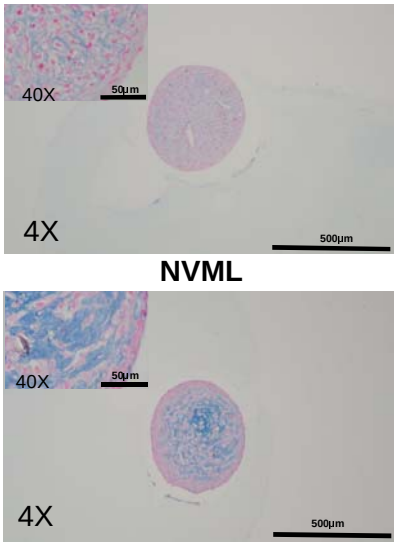

F

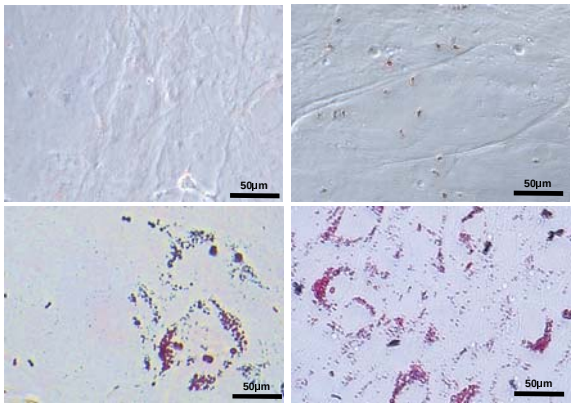

G

Figure.4

A

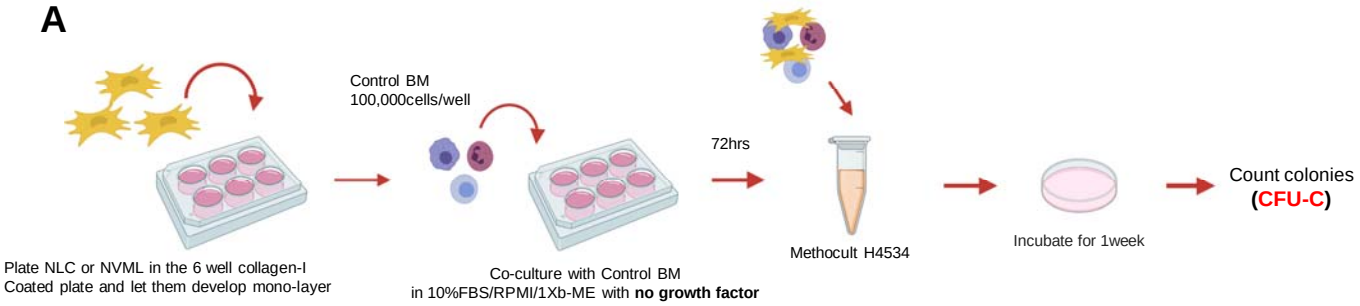

B

+Control BM

C

*

**

***

***

*

**

**

Figure.5

A

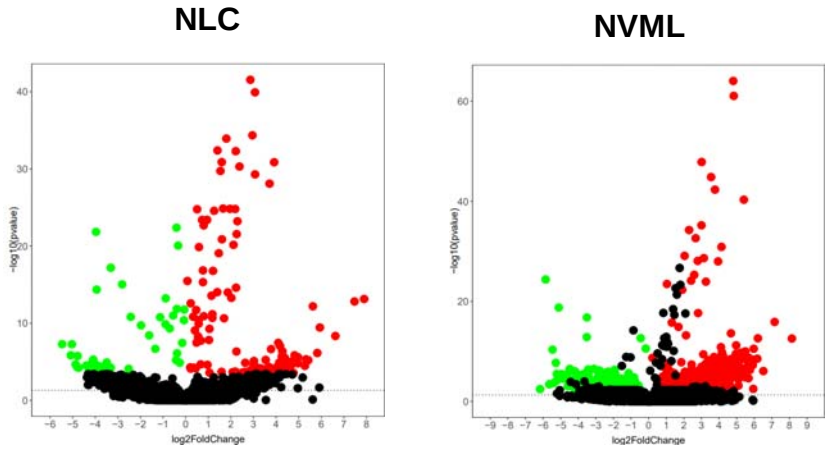

B

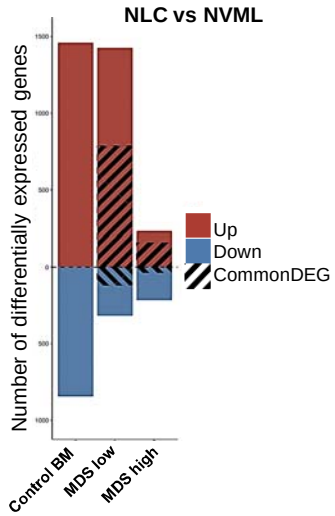

C

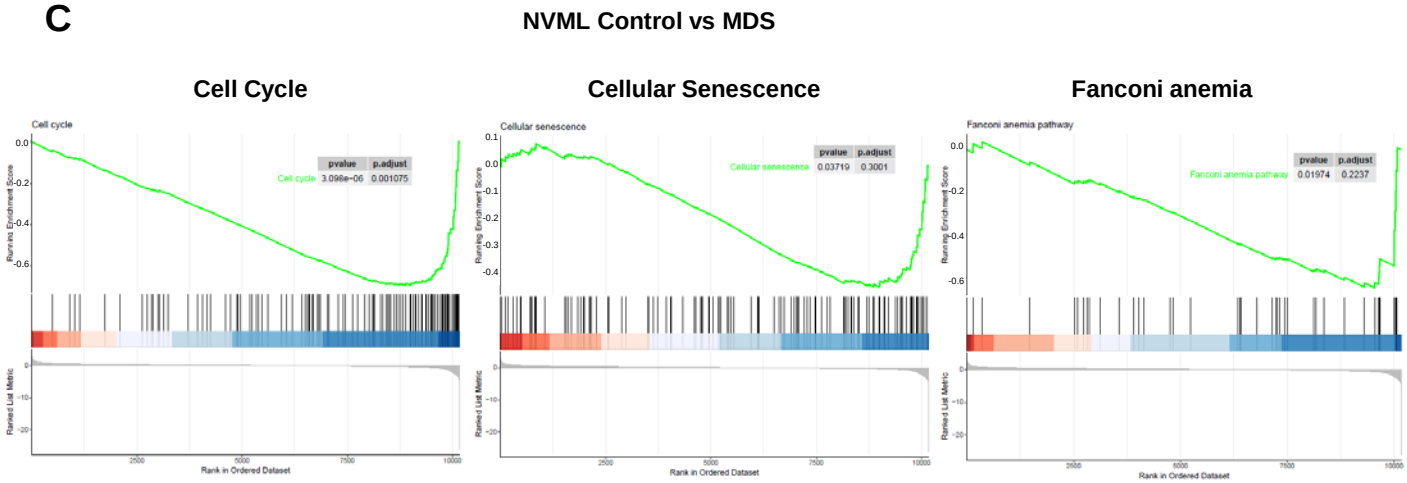

D

E

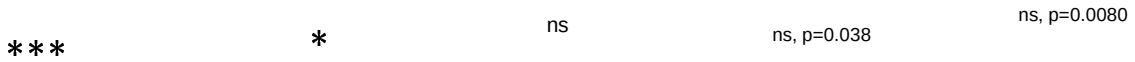

Figure.6

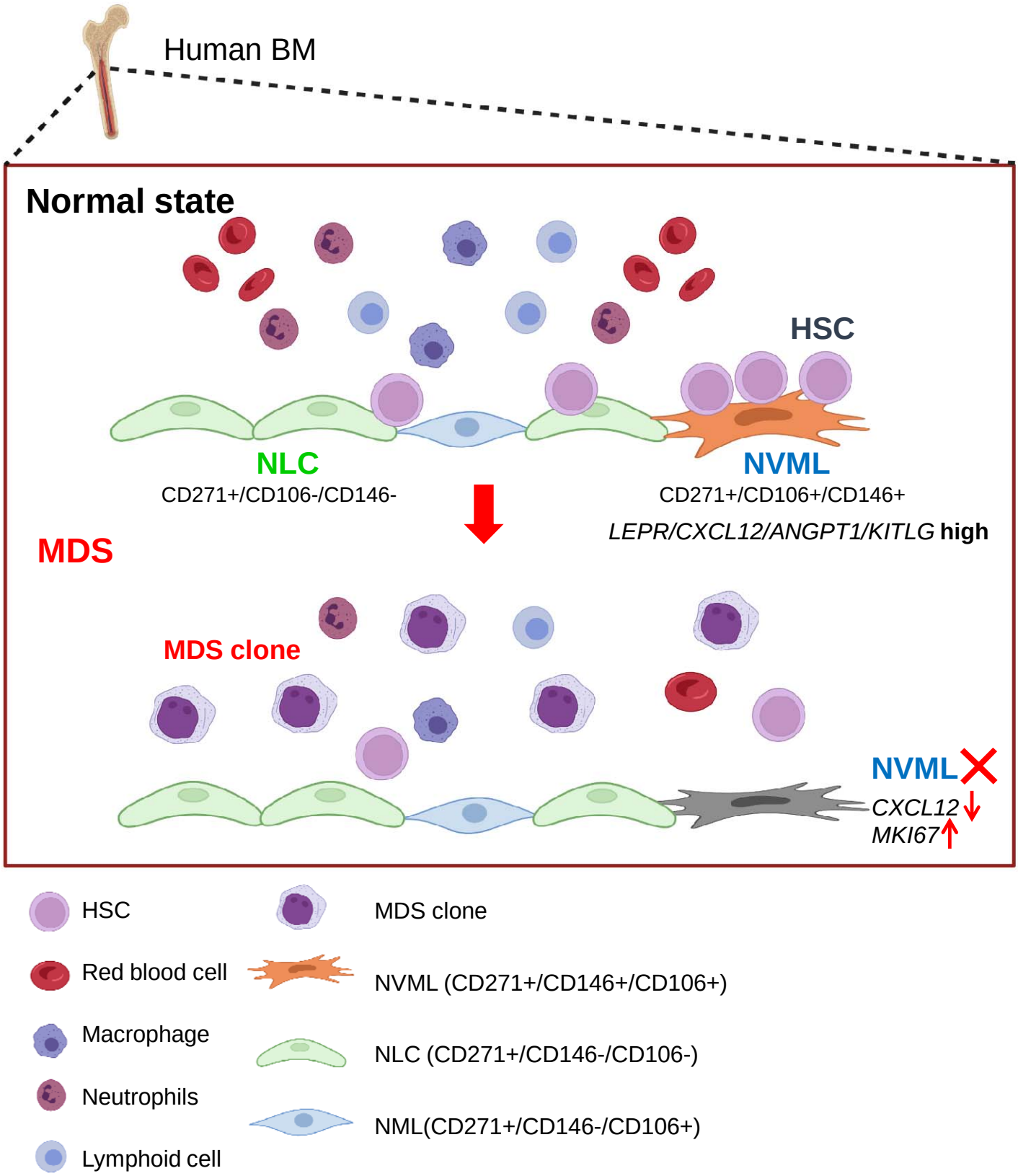
Human BM
Normal state
HSC
NLC
CD271+/CD106-/CD146-
NVML
CD271+/CD106+/CD146+
LEPR/CXCL12/ANGPT1/KITLG high
MDS
MDS clone
NVML
CXCL12
MKI67
HSC
Red blood cell
Macrophage
Neutrophils
Lymphoid cell
MDS clone
NVML (CD271+/CD146+/CD106+)
NLC (CD271+/CD146-/CD106-)
NML(CD271+/CD146-/CD106+)